Int. J. Heat Mass Transfer. Vol. 36, No. 5, pp. 1303–1313, 1993
Printed in Great Britain

0017-9310/93 $6.00+0.00
Pergamon Press Ltd

Conjugate problems of conduction and free convection on vertical and horizontal flat plates

WEN-SHING YU and HSIAO-TSUNG LIN†
Department of Chemical Engineering, National Central University, Chungli, Taiwan 32054, Republic of China

(*Received* 23 *October* 1989 *and in final form* 12 *June* 1992)

Abstract—This paper proposes appropriate conjugate parameters, dimensionless coordinates and temperatures to analyze the conjugate problems of heat conduction in solid walls coupled with laminar free convection flows adjacent to vertical and horizontal flat plates. The obtained finite-difference solutions are uniformly valid over the entire thermo-fluid-dynamic field for fluids of any Prandtl number between 0.001 and infinity. The variations of the local heat transfer rates as well as the interface temperatures and frictions along the plates are shown explicitly. Typical velocity and temperature profiles in the boundary layers are presented. Very comprehensive and accurate correlations of the local Nusselt numbers are also presented and are compared with the reported correlation equations for the vertical case.

1. INTRODUCTION

CONJUGATE problems of conduction and free convection along a vertical flat plate have received considerable attention [1–7]. The early theoretical and experimental works of conjugate free convection have been reviewed in refs. [4, 5].

Recently, Pozzi and Lupo [7] have obtained an initial expansion solution and improved the asymptotic expansion solution of Timma and Padet [6] by adding higher order terms. The initial and asymptotic expansions were based on the features of conjugate problems that the thermo-fluid-dynamic fields near the leading- and the trailing-edge of the plate are that of the constant heat flux and the constant temperature cases, respectively [7]. These features of conjugate problems have been confirmed by the authors [8] using a scale analysis on the heat flux continuity equation at the solid–fluid interface.

In this paper, we propose new conjugation parameters and novel dimensionless coordinates and temperatures to solve the conjugate free convection on a vertical plate. The definitions of these variables reflect the conjugate problem as a hybrid system of ordinary free convection with constant wall temperature and that with constant wall heat flux. All of the defined dimensionless variables are appropriate over the entire thermo-fluid-dynamic field for fluids of any Prandtl number between 0.001 and infinity. For the extremely large and small values of conjugation parameter, the variables and the transformed nonsimilar equations of the conjugate-free convection are readily reducible to those of the ordinary free convection with boundary conditions of constant wall heat flux and constant wall temperature, respectively. From the physically more strict analysis, we are able to obtain very accurate finite-difference solutions over the entire regions of conjugation parameter and Prandtl number. Moreover, a very simple, but very comprehensive and accurate, correlation of the local Nusselt number can be derived in terms of the proper dimensionless variables.

The conjugate free convection over a horizontal flat plate is also studied in this paper by a similar procedure of analysis. To the knowledge of the authors, this conjugate problem has never been reported.

2. SYSTEM EQUATIONS

The schematic diagrams and coordinate systems for the conjugate problems of a vertical and a horizontal flat plates are shown in Figs. 1(a) and (b), respectively. The inner surface of each plate is kept at a constant temperature T_b. Outside the plate, there is the quiescent ambient fluid at a lower constant temperature T_∞. Heat is transferred steadily by conduction in the solid wall coupled with free convection in the fluid. As had been pointed out in ref. [5], axial heat conduction in the flat plate is insignificant. Consequently, the temperature profile in the plate can be assumed to be linear [6, 7].

In the conjugate problems, conduction and convection are coupled by the heat flux continuity condition at the solid–fluid interface [6, 7]

$$-k_f\left(\frac{\partial T}{\partial Y}\right)_{y=0} = k_s(T_b - T_0)/b. \qquad (1)$$

Unlike the ordinary free convection, the interface tem-

† Author to whom all correspondence should be addressed.

NOMENCLATURE

b	plate thickness
f	reduced stream function
g	gravitational acceleration
h	local heat transfer coefficient
k	thermal conductivity
Nu	local Nusselt number, hx/k_f
p	pressure
Pr	Prandtl number
q	heat flux
q_h	$k_s(T_b-T_\infty)/b$
q_t	$h_t(T_b-T_\infty)$
Ra_h	local Rayleigh number, $g\beta(q_h x/k_f)x^3/\alpha\nu$
Ra_t	local Rayleigh number, $g\beta(T_b-T_\infty)x^3/\alpha\nu$
T	temperature
T_b	temperature at the inner surface of the plate
T^*	dimensionless temperature, $(T-T_\infty)/(T_b-T_\infty)$
u	velocity component in x-direction
v	velocity component in y-direction
x	coordinate parallel to the plate
X	dimensionless group defined by equation (76)
y	coordinate normal to the plate
Y	Nu/Nu_h.

Greek symbols

α	thermal diffusivity
β	thermal expansion coefficient
δ	thermal boundary layer thickness
ζ	conjugation parameter, $(k_f b/k_s x)\lambda$
η	dimensionless coordinate, $(y/x)\lambda$
θ	dimensionless temperature $(T-T_\infty)/(T_b-T_\infty)+[(T-T_\infty)/(q_h x/k_f)](\sigma Ra_h)^n$ with $n = 1/5$ for vertical plate and $n = 1/6$ for horizontal plate
λ	$[(\sigma Ra_t)^{-1}+(\sigma Ra_h)^{-4/5}]^{-1/4}$ for vertical plate and $[(\sigma Ra_t)^{-1}+(\sigma Ra_h)^{-5/6}]^{-1/5}$ for horizontal plate
ν	kinematic viscosity
ξ	dimensionless x-coordinate, $[1+\sigma Ra_t/(\sigma Ra_h)^{4/5}]^{-1}$ for vertical plate and $[1+\sigma Ra_t/(\sigma Ra_h)^{5/6}]^{-1}$ for horizontal plate
ρ	fluid density
σ	$Pr/(1+Pr)$
τ	shear stress
ϕ	angle of inclination measured from the horizontal
ψ	stream function
ω	dimensionless pressure, $\sigma p x^2/\rho\alpha\nu\lambda^4$.

Subscripts

f	fluid
h	case of constant wall heat flux
s	solid wall
t	case of constant wall temperature
0	at the solid–fluid interface
∞	beyond the boundary layer.

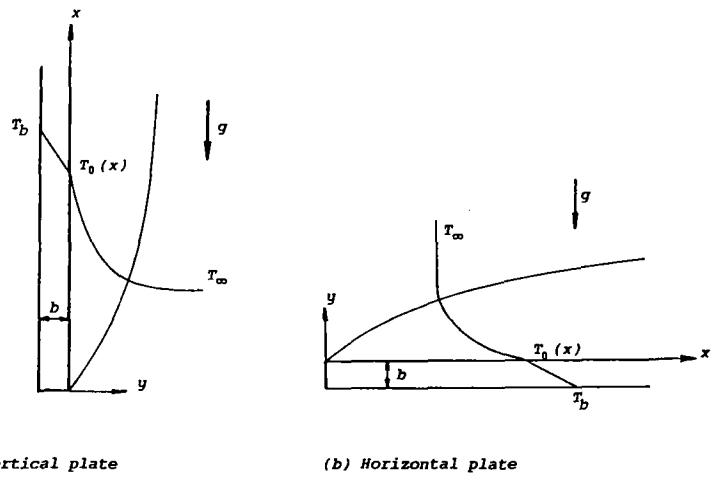

FIG. 1. Schematic diagram and coordinate system of the conjugate problems: (a) vertical plate, and (b) horizontal plate.

perature $T_0(x)$ in conjugate-free convection is not known *a priori* but depends on the location and the intrinsic properties of the system as well as the temperature difference $(T_b - T_\infty)$.

The interface temperature can be determined from the following laminar boundary-layer equations

$$\frac{\partial u}{\partial x} + \frac{\partial v}{\partial y} = 0 \tag{2}$$

$$u\frac{\partial u}{\partial x} + v\frac{\partial u}{\partial y} = -\frac{1}{\rho}\frac{\partial p}{\partial x} + \nu\frac{\partial^2 u}{\partial y^2} + g\beta(T - T_\infty)\sin\phi \tag{3}$$

$$0 = -\frac{1}{\rho}\frac{\partial p}{\partial y} + g\beta(T - T_\infty)\cos\phi \tag{4}$$

$$u\frac{\partial T}{\partial x} + v\frac{\partial T}{\partial y} = \alpha\frac{\partial^2 T}{\partial y^2}. \tag{5}$$

For a horizontal plate, the angle ϕ to the horizontal is 0, while for a vertical plate, $\phi = \pi/2$. In addition, $\partial p/\partial x$ and $\partial p/\partial y$ are equal to zero for a vertical plate. In formulating equations (2)–(5), viscous dissipation and compression work have been neglected. Moreover, physical properties of the fluid are assumed to be constant except for the density variation that induces the buoyancy force.

Equations (2)–(5) are subjected to the boundary conditions of equation (1) and

$$u = 0, \quad v = 0, \quad \text{at} \quad y = 0; \tag{6}$$

$$u = 0, \quad p = 0, \quad T = T_\infty, \quad \text{as} \quad y \to \infty. \tag{7}$$

3. VARIABLES AND FORMULATIONS FOR A VERTICAL PLATE

From a scale analysis on equation (1), we have

$$\frac{T_b - T_0}{T_0 - T_\infty} \sim \frac{k_f b}{k_s \delta(x)} \equiv \zeta \tag{8}$$

where the thermal boundary layer thickness $\delta(x)$ at the location x depends on the thermo-fluid-dynamic of the system. The conjugation parameter ζ, which controls the characteristics of the conjugate problems, is physically the ratio of the conduction resistance in solid to the convection resistance in fluid.

For the extreme case of $\zeta \to 0$, it yields $T_0 \cong T_b$ from equation (8). In this case, the thermo-fluid-dynamic field is that of the conventional isothermal plate flow. Therefore, one has [9]

$$\delta_t(x) \sim x(\sigma Ra_t)^{-1/4} \tag{9}$$

where

$$\sigma = Pr/(1 + Pr) \tag{10}$$

and the local Rayleigh number

$$Ra_t = g\beta(T_b - T_\infty)x^3/\alpha\nu. \tag{11}$$

For the other extreme case of $\zeta \to \infty$, equation (8) indicates that $(T_0 - T_\infty) \ll (T_b - T_0)$, and consequently $(T_b - T_0) \cong (T_b - T_\infty)$. In this case, the present conjugate problem reduces to the traditional free convection on a plate of constant wall heat flux, since equation (1) can be reduced to

$$-k_f\left(\frac{\partial T}{\partial y}\right)_{y=0} = k_s(T_b - T_\infty)/b = \text{constant}. \tag{12}$$

The thermal boundary layer thickness for this extreme case scales is

$$\delta_h(x) \sim x(\sigma Ra_h)^{-1/5} \tag{13}$$

where

$$Ra_h = g\beta(q_h x/k_f)x^3/\alpha\nu \tag{14}$$

is the local Rayleigh number for a plate with constant wall heat flux

$$q_h = k_s(T_b - T_\infty)/b. \tag{15}$$

It is worth noting that

$$Ra_t/Ra_h = k_f b/k_s x. \tag{16}$$

The thermal boundary layer thickness of the conjugate-free convection would be a combination of the thicknesses δ_t and δ_h of the extreme cases. We propose that

$$\delta(x) \sim [\delta_t^4 + \delta_h^4]^{1/4} \sim x/\lambda \tag{17}$$

were

$$\lambda = [(\sigma Ra_t)^{-1} + (\sigma Ra_h)^{-4/5}]^{-1/4}. \tag{18}$$

From equations (8) and (17), the conjugation parameter for the conjugate-free convection on a vertical plate becomes

$$\begin{aligned}\zeta &= (k_f b/k_s x)\lambda \\ &= (k_f b/k_s x)(\sigma Ra_t)^{1/4}[1 + \sigma Ra_t/(\sigma Ra_h)^{4/5}]^{-1/4} \\ &= [(\sigma Ra_t)^{5/4}/\sigma Ra_h][1 + \sigma Ra_t/(\sigma Ra_h)^{4/5}]^{-1/4}.\end{aligned} \tag{19}$$

Based on the foregoing analysis, we introduce the following dimensionless coordinates

$$\eta(x, y) = y/\delta(x) = (y/x)\lambda \tag{20}$$

and

$$\xi(x) = [1 + \sigma Ra_t/(\sigma Ra_h)^{4/5}]^{-1}. \tag{21}$$

In addition, we propose a novel dimensionless temperature

$$\begin{aligned}\theta(\xi, \eta) &= \frac{T - T_\infty}{T_b - T_\infty} + \frac{T - T_\infty}{q_h x/k}(\sigma Ra_h)^{1/5} \\ &= \frac{T - T_\infty}{T_b - T_\infty}\left[1 + \frac{k_f b}{k_s x}(\sigma Ra_h)^{1/5}\right] \\ &= \frac{T - T_\infty}{T_b - T_\infty}\left[1 + \frac{Ra_t}{Ra_h}(\sigma Ra_h)^{1/5}\right] \\ &= \frac{T - T_\infty}{T_b - T_\infty}\xi^{-1}\end{aligned} \tag{22}$$

and a reduced stream function

$$f(\xi,\eta)=\psi(x,y)/\alpha\lambda. \tag{23}$$

The governing equations along with the boundary conditions for the vertical case are then transformed into

$$Pr\,f'''+\frac{16-\xi}{20}ff''-\frac{6-\xi}{10}f'f'+(1+Pr)\theta = \tfrac{1}{5}\xi(1-\xi)\left[f'\frac{\partial f'}{\partial\xi}-f''\frac{\partial f}{\partial\xi}\right] \tag{24}$$

$$\theta''+\frac{16-\xi}{20}f\theta'-\frac{1-\xi}{5}f'\theta=\tfrac{1}{5}\xi(1-\xi)\left[f'\frac{\partial\theta}{\partial\xi}-\theta'\frac{\partial f}{\partial\xi}\right] \tag{25}$$

$$\xi\theta(\xi,0)-(1-\xi)^{5/4}\theta'(\xi,0)=1 \tag{26}$$

$$f(\xi,0)=0,\quad f'(\xi,0)=0 \tag{27}$$

$$f'(\xi,\infty)=0,\quad \theta(\xi,\infty)=0. \tag{28}$$

From equations (24)–(28), the local interface temperature $\theta(\xi, 0)$ can be obtained numerically. The temperature gradient at the interface, $\theta'(\xi,0)$, can then be calculated from equation (26). The local Nusselt number, $Nu=hx/k_f$, can be determined by

$$Nu/\lambda=-\theta'(\xi,0)/\theta(\xi,0) \tag{29}$$

or

$$Nu/\lambda=\frac{1-\xi\theta(\xi,0)}{(1-\xi)^{5/4}\theta(\xi,0)}. \tag{30}$$

It is worth mentioning that the preceding definitions of the key transformation variables λ and ξ are not unique for the analysis of conjugate-free convection. However, by using the present definitions, the transformed equations, the expression of the local Nusselt number, and the derived correlation of the numerical results are the simplest ones in form.

The dimensionless streamwise coordinate $\xi(x)$ is also an alternative form of the conjugation parameter. It relates to ζ by

$$\zeta=(1-\xi)^{5/4}/\xi. \tag{31}$$

For the limiting case of $\xi=0$ ($\zeta\to\infty$), equations (24)–(26) and (29) are reduced to the following similar equations of the ordinary free convection on a plate of constant wall heat flux:

$$Pr\,f'''+\tfrac{4}{5}ff''-\tfrac{3}{5}f'f'+(1+Pr)\theta=0 \tag{32}$$

$$\theta''+\tfrac{4}{5}f\theta'-\tfrac{1}{5}f'\theta=0 \tag{33}$$

$$\theta'(0,0)=-1 \tag{34}$$

and

$$Nu_h/(\sigma Ra_h)^{1/5}=1/\theta(0,0). \tag{35}$$

For the other limiting case of $\xi=1$ ($\zeta=0$), the equations are reduced to

$$Pr\,f'''+\tfrac{3}{4}ff''-\tfrac{1}{2}f'f'+(1+Pr)\theta=0 \tag{36}$$

$$\theta''+\tfrac{3}{4}f\theta'=0 \tag{37}$$

$$\theta(1,0)=1 \tag{38}$$

and

$$Nu_t/(\sigma Ra_t)^{1/4}=-\theta'(1,0). \tag{39}$$

Equations (36)–(39) are equivalent to the equations of the nonconjugate-free convection on an isothermal flat plate [9].

4. VARIABLES AND FORMULATIONS FOR A HORIZONTAL PLATE

Following a similar procedure of the preceding analysis for the vertical plate, we propose

$$\lambda=x/\delta(x)=[(\sigma Ra_t)^{-1}+(\sigma Ra_h)^{-5/6}]^{-1.5} \tag{40}$$

for defining the conjugation parameter ζ, the dimensionless coordinate η, and the reduced stream function $f(\xi,\eta)$ of the conjugate-free convection on a horizontal flat plate. The dimensionless x-coordinate and the dimensionless temperature for the horizontal plate are defined, respectively, as

$$\xi(x)=[1+\sigma Ra_t/(\sigma Ra_h)^{5/6}]^{-1} \tag{41}$$

$$\theta(\xi,\eta)=\frac{T-T_\infty}{T_h-T_\infty}+\frac{T-T_\infty}{q_h x/k_f}(\sigma Ra_h)^{1/6} =\frac{T-T_\infty}{T_h-T_\infty}\left[1+\frac{Ra_t}{Ra_h}(\sigma Ra_h)^{1/6}\right] =\frac{T-T_\infty}{T_h-T_\infty}\xi^{-1}. \tag{42}$$

Moreover, a dimensionless pressure is defined as

$$\omega(\xi,\eta)=\sigma p x^2/\rho\alpha\nu\lambda^4. \tag{43}$$

With these dimensionless variables, the transformed equations for the horizontal case are derived as

$$Pr\,f'''+\frac{10-\xi}{15}ff''-\frac{5-2\xi}{15}f'f' +\tfrac{1}{15}(1+Pr)[(5+\xi)\eta\omega'-(10-4\xi)\omega] =\tfrac{1}{3}\xi(1-\xi)\left[f'\frac{\partial f'}{\partial\xi}-f''\frac{\partial f}{\partial\xi}+(1+Pr)\frac{\partial\omega}{\partial\xi}\right] \tag{44}$$

$$\theta=\omega' \tag{45}$$

$$\theta''+\frac{10-\xi}{15}f\theta'-\frac{1-\xi}{3}f'\theta=\tfrac{1}{3}\xi(1-\xi)\left[f'\frac{\partial\theta}{\partial\xi}-\theta'\frac{\partial f}{\partial\xi}\right] \tag{46}$$

$$\xi\theta(\xi,0)-(1-\xi)^{6/5}\theta'(\xi,0)=1 \tag{47}$$

$$f(\xi,0)=0,\quad f'(\xi,0)=0 \tag{48}$$

$$f'(\xi,\infty)=0,\quad \omega(\xi,\infty)=0,\quad \theta(\xi,\infty)=0. \tag{49}$$

In addition, the local Nusselt number for the horizontal case is related to $\theta(\xi, 0)$ by

$$Nu/\lambda = -\theta'(\xi,0)/\theta(\xi,0) = \frac{1-\xi\theta(\xi,0)}{(1-\xi)^{6/5}\theta(\xi,0)}. \quad (50)$$

For the limiting case of $\xi = 0$, the nonsimilar equations (44) and (46) as well as equations (47) and (50) are readily reduced to the following equations

$$Pr\, f''' + \tfrac{2}{3} f f'' - \tfrac{1}{3} f' f' + \tfrac{1}{3}(1+Pr)(\eta\omega' - 2\omega) = 0 \quad (51)$$

$$\theta'' + \tfrac{2}{3} f\theta' - \tfrac{1}{3} f'\theta = 0 \quad (52)$$

$$\theta'(0,0) = -1 \quad (53)$$

and

$$Nu_h/(\sigma Ra_h)^{1/6} = 1/\theta(0,0). \quad (54)$$

While for the other limiting case of $\xi = 1$, the reduced equations are

$$Pr\, f''' + \tfrac{3}{5} f f'' - \tfrac{1}{5} f' f' + \tfrac{2}{5}(1+Pr)(\eta\omega' - \omega) = 0 \quad (55)$$

$$\theta'' + \tfrac{3}{5} f\theta' = 0 \quad (56)$$

$$\theta(1,0) = 1 \quad (57)$$

and

$$Nu_t/(\sigma Ra_t)^{1/5} = -\theta'(1,0). \quad (58)$$

5. NUMERICAL METHOD

The set of nonsimilar equations (24)–(28) for the vertical case and that of equations (44)–(49) for the horizontal case are solved by Keller's finite-difference scheme known as the box method [10]. The numerical integration was carried out step-by-step from $\xi = 0$ to 1 with uniform step size $\Delta\xi = 0.01$. However, the step size $\Delta\eta$ and the edge of the boundary layer, η_∞, were varied with different Prandtl number for obtaining converged accurate solutions. We used variable step size $\Delta\eta_i = 1.02\Delta\eta_{i-1}$ with $\Delta\eta_0 = 0.002$ for small Prandtl numbers ($Pr \leqslant 0.1$) and $\Delta\eta_0 = 0.005$ for large Prandtl numbers ($Pr \geqslant 100$). For moderate Prandtl numbers ($Pr = 0.7$ and 7), a uniform step size $\Delta\eta = 0.05$ was used. The edge of the boundary layer, η_∞, was taken as 12 for $Pr \leqslant 0.1$, 15 for $Pr = 0.7$ and 7, and 50 for $Pr \geqslant 100$.

6. RESULTS AND DISCUSSIONS

6.1. *Velocity and temperature profiles*

Typical profiles of the dimensionless longitudinal velocity $f'(\xi, \eta) = u/(\alpha/x)\lambda^2$ for $Pr = 0.7$ are shown in Figs. 2(a) and (b) for the vertical and the horizontal cases, respectively. As shown in these figures, the maximum velocity decreases as ξ increases from 0 to 1.

Typical profiles of the dimensionless temperature $\theta(\xi, \eta)$ are presented in Fig. 3 for $Pr = 0.7$. The profiles of the traditional expression of dimensionless temperature [6, 7]

$$T^* = \frac{T - T_\infty}{T_h - T_\infty} = \xi\theta(\xi,\eta) \quad (59)$$

are plotted in Fig. 4. This figure shows clearly that the interface temperature increases from T_∞ at $\xi = 0$ to T_h at $\xi = 1$.

Figures 2–4 also show a step-by-step variation of the dimensionless velocity and temperature profiles with ξ. It is seen that these profiles develop from the profiles of the constant wall heat flux case ($\xi = 0$) to those of the constant wall temperature case ($\xi = 1$).

6.2. *Interface temperature and shear stress*

Finite-difference solutions of the dimensionless interface temperature $\theta(\xi, 0)$ for various ξ and Pr are listed in Table 1. The numerical results of the dimensionless velocity gradient at the solid–fluid interface, $f''(\xi, 0)$, are listed in Table 2. These tables clearly show that $\theta(\xi, 0)$ and $f''(\xi, 0)$ decrease as ξ increases.

The accuracy of the present numerical results can be verified by comparing with the initial and asymptotic expansions of Pozzi and Lupo [7]. Comparisons are made in Fig. 5 for the dimensionless interface temperature

$$T_0^* = (T_0 - T_\infty)/(T_h - T_\infty) = \xi\theta(\xi,0) \quad (60)$$

and in Fig. 6 for the dimensionless friction at the interface, $\tau_0/\rho(\alpha\nu/x)Ra_t^{3/4}$. As can be seen in these figures, the initial expansion solutions (18 terms) coincide excellently with the present finite-difference solutions for large values of ζ (small values of ξ or x). While the asymptotic expansion solutions (four terms) are in excellent agreement with our results for small values of ζ (large values of ξ or x). The parameters m and m_1 in ref. [7] had been converted to ζ by

$$\zeta = m^{4/5}[Pr^2/(1+Pr)]^{1/5} = m_1^{-1}[Pr^2/(1+Pr)]^{1/5}. \quad (61)$$

The variations of the dimensionless interface temperature

$$\frac{T_h - T_0}{T_h - T_\infty} = 1 - T_0^* = 1 - \xi\theta(\xi,0) \quad (62)$$

with respect to $1/\zeta$ are presented in Fig. 7. It is seen that the interface temperature increases with decreasing ζ. As has also been indicated in Fig. 4, the interface temperature increases from T_∞ as $\zeta \to \infty (\xi = 0$ or $x = 0)$ to T_h at $\zeta = 0$ ($\xi = 1$, $x/b \to \infty$).

Figures 8(a) and (b) show the variations of the dimensionless interface frictions

$$\tau_0/\rho(\alpha\nu/x^2)Ra_t^{3/4} = (\sigma\xi)^{3/4} f''(\xi,0) \quad (63a)$$

and

$$\tau_0/\rho(\alpha\nu/x^2)Ra_t^{3/5} = (\sigma\xi)^{3/5} f''(\xi,0) \quad (63b)$$

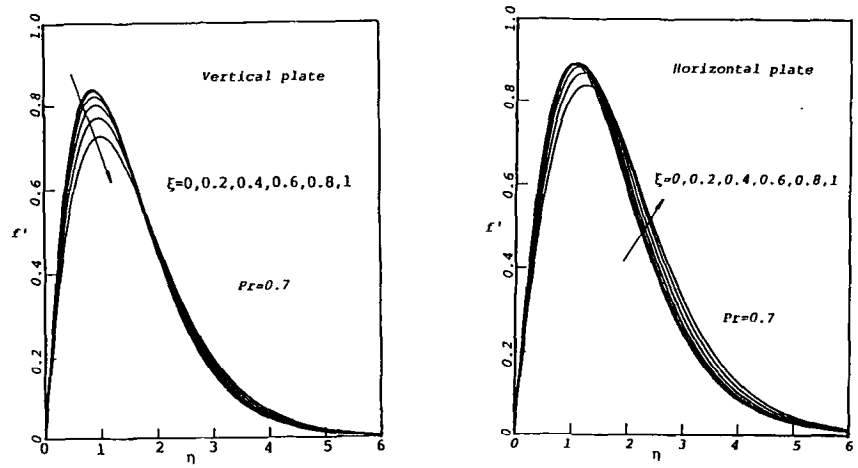

FIG. 2. Typical profiles of the dimensionless longitudinal velocity $f''(\xi, \eta)$ for $Pr = 0.7$.

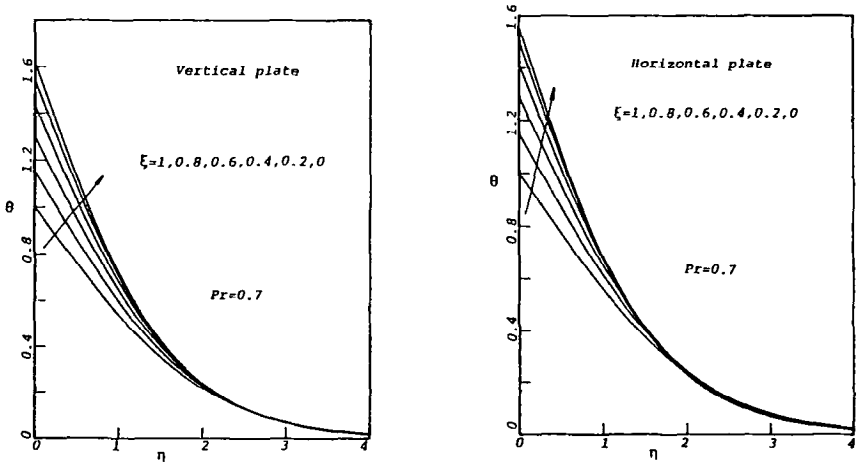

FIG. 3. Typical profiles of the dimensionless temperature $\theta(\xi, \eta)$ for $Pr = 0.7$.

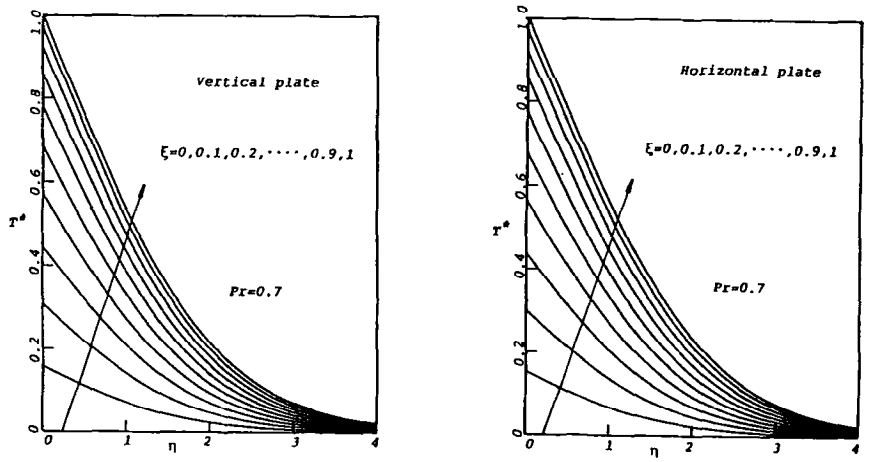

FIG. 4. Typical profiles of the dimensionless temperature T^* for $Pr = 0.7$.

Table 1. Numerical results of $\theta(\xi, 0)$

ξ	0.001	0.01	0.1	Pr 0.7	7	100	∞
(a) *Vertical plate*							
0	1.3345	1.3759	1.4824	1.6132	1.6520	1.6108	1.5868
0.1	1.3364	1.3731	1.4664	1.5783	1.6102	1.5745	1.5538
0.2	1.3321	1.3637	1.4430	1.5358	1.5611	1.5310	1.5136
0.3	1.3206	1.3468	1.4116	1.4858	1.5049	1.4805	1.4664
0.4	1.3007	1.3215	1.3721	1.4286	1.4424	1.4234	1.4124
0.5	1.2717	1.2872	1.3246	1.3652	1.3746	1.3606	1.3525
0.6	1.2335	1.2442	1.2698	1.2970	1.3029	1.2933	1.2877
0.7	1.1865	1.1932	1.2090	1.2255	1.2289	1.2229	1.2194
0.8	1.1319	1.1354	1.1436	1.1522	1.1538	1.1506	1.1488
0.9	1.0705	1.0718	1.0748	1.0778	1.0784	1.0772	1.0766
1.0	1.0000	1.0000	1.0000	1.0000	1.0000	1.0000	1.0000
(b) *Horizontal plate*							
0	1.2258	1.2720	1.3944	1.5583	1.6410	1.6230	1.6081
0.1	1.2409	1.2826	1.3913	1.5333	1.6022	1.5859	1.5729
0.2	1.2511	1.2876	1.3814	1.5003	1.5558	1.5414	1.5302
0.3	1.2549	1.2857	1.3634	1.4590	1.5017	1.4894	1.4802
0.4	1.2504	1.2751	1.3364	1.4095	1.4406	1.4306	1.4233
0.5	1.2361	1.2546	1.2998	1.3523	1.3735	1.3657	1.3603
0.6	1.2103	1.2231	1.2538	1.2885	1.3019	1.2963	1.2926
0.7	1.1728	1.1807	1.1993	1.2200	1.2276	1.2240	1.2216
0.8	1.1245	1.1285	1.1380	1.1485	1.1522	1.1502	1.1490
0.9	1.0671	1.0686	1.0720	1.0757	1.0770	1.0762	1.0758
1.0	1.0000	1.0000	1.0000	1.0000	1.0000	1.0000	1.0000

for the vertical and horizontal plates, respectively. These figures reveal that the dimensionless interface frictions increase as ζ decreases, or equivalently, as ξ or x increases.

6.3. *Local heat transfer rates*

In the conjugate problems, the local heat transfer rate cannot be evaluated from the calculated local Nusselt number or heat transfer coefficient alone,

Table 2. Numerical results of $f''(\xi, 0)$

ξ	0.001	0.01	0.1	Pr 0.7	7	100	∞
(a) *Vertical plate*							
0	54.745	16.929	5.2502	2.3123	1.5745	1.5248	1.5419
0.1	55.050	16.982	5.2335	2.2872	1.5537	1.5079	1.5269
0.2	55.193	16.981	5.1988	2.2542	1.5276	1.4861	1.5069
0.3	55.136	16.917	5.1440	2.2127	1.4960	1.4591	1.4816
0.4	54.840	16.778	5.0669	2.1625	1.4591	1.4267	1.4508
0.5	54.268	16.556	4.9664	2.1040	1.4171	1.3891	1.4146
0.6	53.392	16.245	4.8424	2.0377	1.3705	1.3467	1.3732
0.7	52.199	15.843	4.6961	1.9646	1.3199	1.3000	1.3272
0.8	50.692	15.353	4.5294	1.8859	1.2660	1.2494	1.2769
0.9	48.869	14.776	4.3431	1.8018	1.2090	1.1951	1.2224
1.0	46.595	14.073	4.1270	1.7083	1.1460	1.1340	1.1605
(b) *Horizontal plate*							
0	47.166	14.549	4.5424	2.0205	1.3622	1.2958	1.2987
0.1	47.190	14.521	4.5068	1.9902	1.3383	1.2754	1.2797
0.2	47.051	14.439	4.4544	1.9529	1.3102	1.2513	1.2570
0.3	46.710	14.295	4.3832	1.9084	1.2780	1.2235	1.2306
0.4	46.125	14.077	4.2914	1.8569	1.2421	1.1921	1.2008
0.5	45.290	13.777	4.1786	1.7989	1.2030	1.1578	1.1677
0.6	44.098	13.393	4.0462	1.7356	1.1614	1.1209	1.1320
0.7	42.653	12.933	3.8977	1.6687	1.1181	1.0822	1.0943
0.8	40.984	12.415	3.7386	1.6000	1.0741	1.0423	1.0551
0.9	39.177	11.867	3.5750	1.5308	1.0298	1.0015	1.0147
1.0	37.289	11.301	3.4075	1.4603	0.9839	0.9584	0.9716

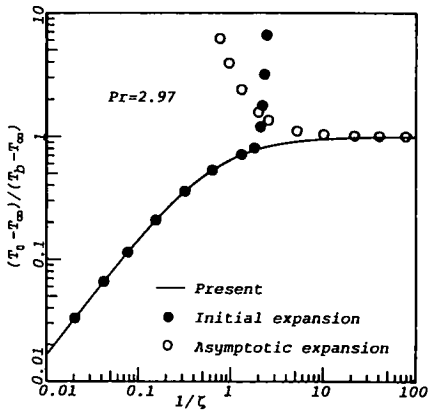

FIG. 5. A comparison of the dimensionless interface temperature along the vertical plate, $Pr = 2.97$.

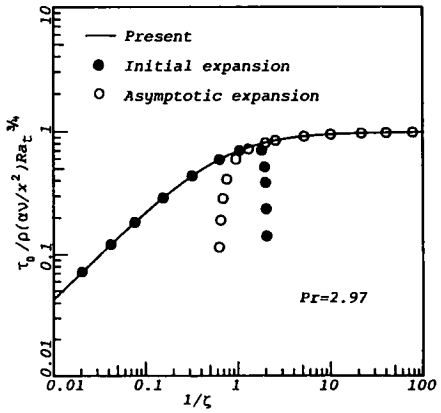

FIG. 6. A comparison of the dimensionless interface friction along the vertical plate, $Pr = 2.97$.

since the interface temperature is unspecified. The local heat transfer rate can be evaluated, only after $\theta(\xi, 0)$ has been determined by

$$q = k_s(T_h - T_0)/b$$
$$= (k_s/b)(T_h - T_\infty)\left[1 - \frac{T_0 - T_\infty}{T_h - T_\infty}\right]$$
$$= q_h[1 - \xi\theta(\xi, 0)]. \quad (64)$$

Figure 7 presents the variations of the dimensionless heat transfer rate q/q_h with ζ and Pr. It is seen that the local heat transfer rate decreases as ζ decreases (ξ or x increases). The decrease of the local heat transfer rate is due to the increase of the thermal boundary layer thickness.

The local heat transfer rate can also be calculated from

$$q = h(T_0 - T_\infty)$$
$$= Nu\frac{k_f}{x}(T_h - T_\infty)\xi\theta(\xi, 0) \quad (65)$$

where the local Nusselt number can be calculated from equation (30) for the vertical case and from equation (50) for the horizontal case. It can also be estimated from the correlation equations presented in the next section.

Equation (65) can be rewritten as

$$q/q_l = [\theta'(\xi, 0)/\theta'(1, 0)]\xi \quad (66)$$

where

$$q_l = h_l(T_h - T_\infty) = Nu_l(k_f/x)(T_h - T_\infty) \quad (67)$$

is the local heat transfer rate of the ordinary free convection on an isothermal plate. The local Nusselt number of an isothermal plate, Nu_l, can be calculated from equation (39) for the vertical plate and equation (58) for the horizontal plate with $\theta'(1, 0)$ reported in ref. [11].

The heat transfer rate varies from an asymptote of $q = q_h$ to the other asymptote of $q = q_l$ as the conjugate parameter ζ varies from infinity to 0. For very small and large values of ζ, the solutions of the ordi-

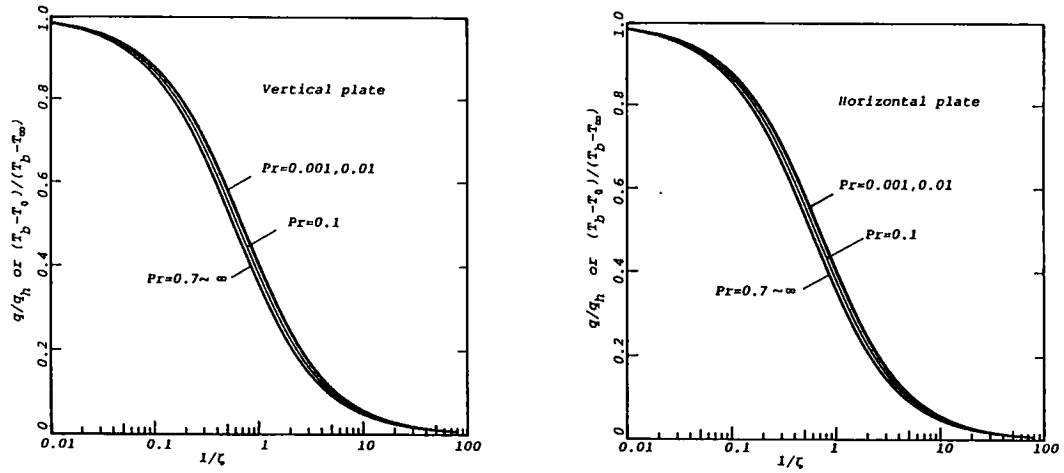

FIG. 7. Variations of the local heat transfer rate and the interface temperature.

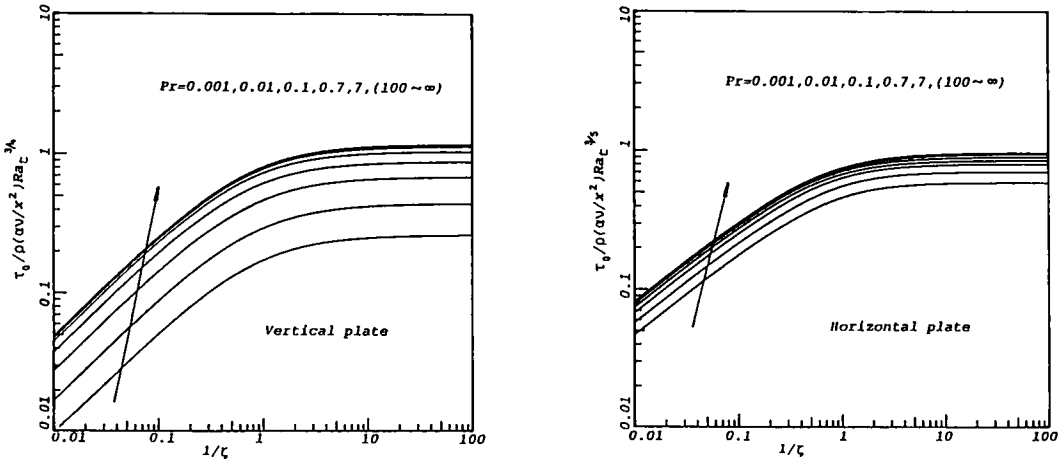

FIG. 8. Variations of the dimensionless interface friction.

nary free convection of constant wall temperature and constant wall heat flux, respectively, can be applied satisfactorily. Table 3 presents the regimes of the conjugation parameter in which a convective system should be solved as a conjugate problem. Beyond these regimes, the free convection system can be approximated by the ordinary ones with error of heat transfer rate to be less than 5%.

Table 3. The regimes of ζ in which a free convection system should be solved as a conjugate problem

Pr	Vertical	Horizontal
0.001	(0.087, 25.5)	(0.146, 23.5)
0.01	(0.089, 26.3)	(0.148, 24.3)
0.1	(0.095, 28.3)	(0.153, 26.7)
0.7	(0.102, 30.8)	(0.159, 29.8)
7	(0.102, 31.6)	(0.157, 31.4)
100	(0.098, 30.7)	(0.151, 31.0)
∞	(0.096, 30.3)	(0.148, 30.8)

6.4. *Local Nusselt number*

The local Nusselt number can be calculated from the numerical results of $\theta(\xi, 0)$ by using equations (30) and (50). Figure 9 shows that Nu/λ decreases almost linearly with increasing ξ for any Prandtl number. This linear relationship should not be taken for granted but is a result of the proper definitions of λ and ξ. The linear relationship between Nu/λ and ξ leads us to propose a simple correlation equation of the local Nusselt number for the conjugate-free convection on a vertical plate

$$Nu/\lambda = \xi[Nu_t/(\sigma Ra_t)^{1/4}] + (1-\xi)[Nu_h/(\sigma Ra_h)^{1/5}] \tag{68}$$

where Nu_t and Nu_h are the local Nusselt numbers of ordinary convective problems with constant wall temperature and constant wall heat flux, respectively. Very accurate (maximum error $<0.5\%$) correlation equations of Nu_t and Nu_h have been proposed by the authors [12] as

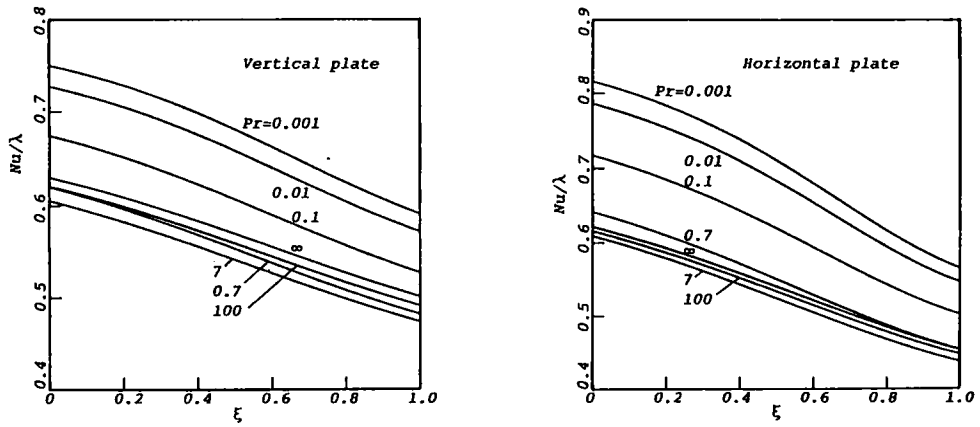

FIG. 9. Variations of Nu/λ with ξ.

$$Nu_t/(\sigma Ra_t)^{1/4} = 0.502\left[\frac{1+Pr}{0.492+0.986Pr^{1/2}+Pr}\right]^{1/4} \quad (69)$$

$$Nu_h/(\sigma Ra_h)^{1/5} = 0.631\left[\frac{1+Pr}{0.396+0.918Pr^{1/2}+Pr}\right]^{1/5} \quad (70)$$

for $0.001 \leqslant Pr \leqslant \infty$.

For a horizontal plate, the correlation equation is proposed as

$$Nu/\lambda = \xi[Nu_t/(\sigma Ra_t)^{1/5}] + (1-\xi)[Nu_h/(\sigma Ra_h)^{1/6}]. \quad (71)$$

The correlations of Nu_t and Nu_h for the nonconjugate-free convection on a horizontal plate have been introduced [12] as

$$Nu_t/(\sigma Ra_t)^{1/5} = 0.456\left[\frac{1+Pr}{0.313+0.856Pr^{1/2}+Pr}\right]^{1/5} \quad (72)$$

$$Nu_h/(\sigma Ra_h)^{1/6} = \left[\frac{1+Pr}{0.177+0.625Pr^{1/2}+Pr}\right]^{1/6}. \quad (73)$$

The maximum discrepancy of the correlation equations (72) and (73) to the numerical data is less than 0.5% for $0.001 \leqslant Pr \leqslant \infty$.

Equations (68) and (71) can be rewritten as

$$Y = X \quad (74)$$

where

$$Y = Nu/Nu_h \quad (75)$$

and

$$X = (1-\xi)^{1/4}\left[\xi\frac{Nu_t/(\sigma Ra)^{1/4}}{Nu_h/(\sigma Ra)^{1/5}} + (1-\xi)\right] \quad (76a)$$

for a vertical plate, or

$$X = (1-\xi)^{1/5}\left[\xi\frac{Nu_t/(\sigma Ra)^{1/5}}{Nu_h/(\sigma Ra)^{1/6}} + (1-\xi)\right] \quad (76b)$$

for a horizontal plate.

Figures 10(a) and (b) compares the proposed correlations and the numerical data for the vertical and the horizontal cases, respectively. These figures have revealed excellent agreement between the correlations and the numerical results. For the case of a vertical plate, the maximum deviation is less than 2.8% for $0.001 \leqslant Pr \leqslant \infty$. While for a horizontal plate, the maximum discrepancy is less than 3% for $0.001 \leqslant Pr \leqslant \infty$.

The correlation equations (68) and (71) of the local Nusselt numbers provide for the estimations of the dimensionless temperature $\theta(\xi, 0)$ by using equations (30) and (50) for the vertical and horizontal cases, respectively. Eventually, the local heat transfer rate can be determined either from equation (64) or equation (65).

6.5. *Comparisons of the correlation equations*

For the vertical plate, a combination of equations (30), (60), (64) and (68) yields

$$(1-T_0^*)/T_0^* = q/(q_h - q) = \zeta[\xi A(Pr) + (1-\xi)B(Pr)] \quad (77)$$

where $A(Pr) = Nu_t(\sigma Ra_t)^{1/4}$ and $B(Pr) = Nu_h/(\sigma Ra_h)^{1/5}$ are given by equations (69) and (70), respectively.

An implicit correlation equation of dimensionless temperature at the interface had been introduced by Miyamoto *et al.* [5], which can be converted in our notation as

$$T_0^* = \left[1 + 0.482\left(\frac{1-\xi}{\xi}\right)^{5/4} T_0^{*1/4}\right]^{-1} \quad (78)$$

for $Pr = 0.7$. Another correlation equation of the local Nusselt number was reported by Timma and Padet [6]. After converting to our notation, their correlation becomes

$$T_0^* = 1 - C_1\left(\frac{1-\xi}{\xi}\right)^{5/4}\left(\frac{1+Pr}{0.952+Pr}\right)^{1/4} \quad (79)$$

where C_1 was listed in Tables 1 and 2 of [6], which depends weakly on the Grashof number, the Prandtl number, the conductivity ratio k_s/k_f, and the ratio of the plate length to the wall thickness.

The correlation equations (78) and (79), with C_1 was taken as 0.473 [6], are compared in Fig. 11 with our correlation equation (77) and numerical results for $Pr = 0.7$. The comparisons reveal that the correlation of Miyamoto *et al.* [5] is in good agreement with our numerical results and correlation. As expected, the correlation of Timma and Padet [6] from an asymptotic expansion solution is coincident with the present results for small values of ζ but not for large ones.

7. CONCLUSIONS

In this paper, we have analyzed the conjugate problems of conduction and free convection on vertical and horizontal flat plates. The horizontal case has not been studied previously. We used a new analysis method developed from a straight insight into the main features of the conjugate-free convection problems.

The present finite-difference solutions have been proved to be very accurate by the comparisons of the obtained dimensionless interface temperature and friction with the reported series expansion solutions for the vertical plate case. The finite-difference solutions are valid uniformly over the entire thermo-fluid-dynamic field for $0.001 \leqslant Pr \leqslant \infty$. We have extended the solutions to the small values of Prandtl number and to the region where the resistances of the wall

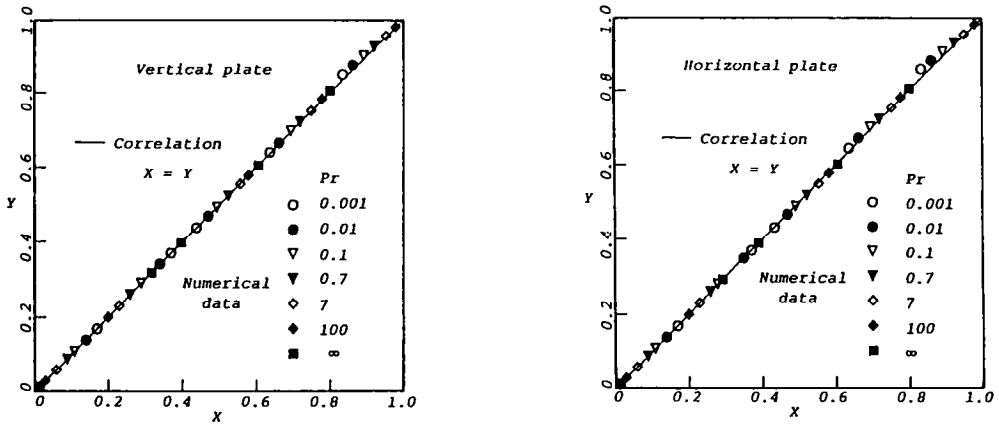

FIG. 10. A comparison between the correlated and the calculated local Nusselt numbers.

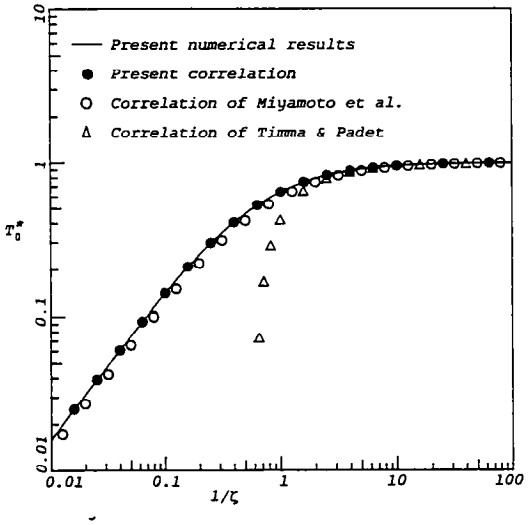

FIG. 11. Comparisons of the correlation equations for the conjugate-free convection on a vertical plate.

conduction and the free convection boundary layer are comparable in magnitude.

For convenience of engineering applications, very accurate correlation equations of the local Nusselt numbers had been derived. From these correlations, the local interface temperature and heat transfer rate can be estimated.

Acknowledgement—The support of the National Science Council, R.O.C. (Grant No. NSC79-0402-E008-11) for this work is gratefully acknowledged.

REFERENCES

1. M. D. Kelleher and K. T. Yang, A steady conjugate heat transfer problem with conduction and free convection, *Appl. Sci. Res.* **17**, 240–268 (1967).
2. A. E. Ziness, The coupling of conduction with laminar natural convection from a vertical flat plate with arbitrary surface heating, *J. Heat Transfer* **92**, 528–535 (1970).
3. K. Chida and Y. Katto, Study on conjugate heat transfer by vectorial dimensional analysis, *Int. J. Heat Mass Transfer* **19**, 453–460 (1976).
4. L. B. Gdalevich and V. E. Fertman, Conjugate problems of natural convection, *J. Engng Phys.* **33**(3), 1120–1126 (1978).
5. M. Miyamoto, J. Sumikawa, T. Akiyoshi and T. Nakamura, Effects of axial heat conduction in a vertical flat plate on free convection heat transfer, *Int. J. Heat Mass Transfer* **23**, 1545–1553 (1980).
6. J. Timma and J. P. Padet, Etude theorique du couplage convection–conduction en convection libre laminaire sur une plaque plane verticale, *Int. J. Heat Mass Transfer* **28**, 1097–1104 (1985).
7. A. Pozzi and M. Lupo, The coupling of conduction with laminar natural convection along a flat plate, *Int. J. Heat Mass Transfer* **31**, 1807–1814 (1988).
8. W.-S. Yu, H.-T. Lin and T.-Y. Hwang, Conjugate heat transfer of conduction and forced convection along wedges and a rotating cone, *Int. J. Heat Mass Transfer* **34**, 2497–2507 (1991).
9. P. S. Larsen and V. S. Arpaci, On the similarity solutions to laminar natural convection boundary layers, *Int. J. Heat Mass Transfer* **29**, 342–344 (1986).
10. T. Cebeci and P. Bradshaw, *Physical and Computational Aspects of Convective Heat Transfer*. Springer, New York (1984).
11. W.-S. Yu and H.-T. Lin, Free convection heat transfer from an isothermal plate with arbitrary inclination, *Wärme- und Stoffübertragung* **23**, 203–211 (1988).
12. H.-T. Lin, W.-S. Yu and C.-C. Chen, Comprehensive correlations for laminar mixed convection on vertical and horizontal flat plates, *Wärme- und Stoffübertragung* **25**, 353–359 (1990).